Evaluations of Weathering of Polar and Nonpolar Petroleum Components in a Simulated Freshwater−Oil Spill by Orbitrap and Fourier Transform Ion Cyclotron Resonance Mass Spectrometry

Chukwuemeka Ajaero, Ian Vander Meulen, Nicole E. Heshka, Qin Xin, Dena W. McMartin,* Kerry M. Peru, Huan Chen, Amy M. McKenna, Kiaura Reed, and John V. Headley

ACCESS | Metrics & More | Article Recommendations | Supporting Information

ABSTRACT: The comprehensive chemical characterization of crude oil is important for the evaluation of the transformation and fate of components in the environment. Molecular-level speciation of naphthenic acid fraction compounds (NAFCs) was investigated in a mesoscale spill tank using both negative-ion electrospray ionization (ESI) Orbitrap mass spectrometry (MS) and positive-ion atmospheric pressure photoionization Fourier transform ion cyclotron resonance mass spectrometry (APPI-FT-ICR-MS). Both ionization techniques are coupled to high-resolution mass spectrometric detectors (ESI: Orbitrap MS; APPI: FT-ICR-MS at 9.4 T), enabling insight into the behavior and fate of petrogenic compounds during a simulated freshwater crude oil spill. Negative-ion ESI Orbitrap-MS reveals that oxygen-containing (O_x) classes are detected early in the spill, whereby species with more oxygen per molecule evolve later in the simulated spill. The O_2-containing species gradually decreased in relative abundance, while O_3 and O_4 species increased in relative abundance throughout the simulated spill, which could correspond to a relative degree of oxygen incorporation. Nonpolar speciation by positive-ion APPI 9.4 T FT-ICR-MS allowed for the identification of water-soluble nonpolar and less polar acidic species. Molecular-level graphical representation of elemental compositions derived from simulated spill water-soluble and oil-soluble species suggest that biological activity is the primary degradation mechanism and that biodegradation was the dominant mechanism based on the negative-ion ESI Orbitrap-MS results.
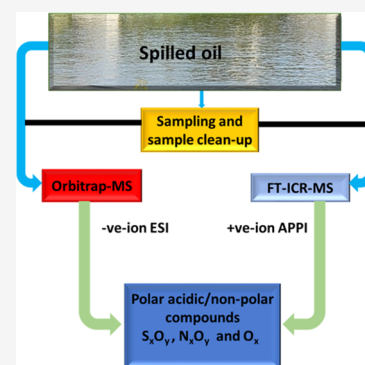
1. INTRODUCTION

Large volumes of crude oil are transported across North America annually. In 2022, approximately 52 billion barrels of crude oil were moved across this region.[1] Accidental spills can occur during various stages of crude oil transportation, consumption, and exploration, such as during the loading and unloading of tankers, pipeline leaks, or accidents involving oil drilling platforms. Such spills of crude oil can pose significant hazards to aquatic environments,[2] including freshwater ecosystems. The average annual accidental release of petroleum into North American marine waters is 260 million liters,[3] which varies from spill to spill and year to year, but typically amounts to tens of thousands of liters.[2] Weathering of oil released into aquatic environments may occur through evaporation, emulsification, dissolution, microbial, and/or photochemical degradation.[4] Most oil-derived compounds are only moderately soluble in water, but some oil-derived substances may become polar from oxidation, effectively enhancing their water solubility. Weathering processes change the chemistry of crude oil and increase its compositional complexity.[5] Many constituents of oil have the potential to be hazardous to marine organisms, but their poor solubility prevents them from being widely bioavailable in the environment. Enhanced solubility of some components increases the

likelihood that molecules can distribute and become bioavailable, resulting in increased environmental prevalence and toxicological significance.[6,7]

The fate and ecotoxicity of spilled crude oil depend on its initial chemical composition and predominant environmental conditions during weathering.[5] For these reasons, understanding the composition of dissolved oil components at the molecular level in freshwater environments is crucial. However, the complexity of petroleum composition makes it extremely challenging to characterize the constituents, which complicates standardizing emergency responses to oil spills.[8] Fourier transform ion cyclotron resonance (FT-ICR) and Orbitrap mass spectrometry (MS) are often applied to crude oil analysis because of their ability to capture wide swathes of a mixture's chemical complexity with ultrahigh resolution and mass accuracy.[9,10] These methods enable unambiguous assignment
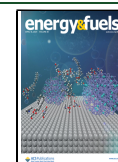
of molecular formulas (e.g., $C_cH_hN_nO_oS_s$) and subsequent classification based on formula heteroatom inclusions,[11,12] size, and unsaturation to obtain a molecular-level characterization of samples.[13−15] Electrospray ionization (ESI) and atmospheric pressure photoionization (APPI) are two frequently employed methods for crude oil studies,[9] and these different ionization techniques are suited to specific classes of compounds. Negative-ion ESI is well suited for characterizing more polar acidic species, while positive-ion APPI is more suited for the characterization of less/nonpolar heteroatom and aromatic species in crude oil.[10] Ion suppression, which makes it simpler to detect easily ionized species (that may not be the most abundant) at the expense of other mixture constituents, is the main challenge in nontarget analysis. A complete sample characterization is made possible by using several ionization techniques, such as ESI and APPI in the negative and positive ionization modes, maybe the solution to this issue.[16,17] The primary reason for the use of APPI in analysis is because of its potential to ionize chemical species that ESI cannot access, thus providing a more detailed composition of the constituents in crude oil.[16,17]

Mesoscale crude oil spill tests in freshwater at different temperatures and durations were simulated by using an indoor spill tank. In a 28-day test using freshwater at a temperature of 15 °C, an increase of unidentified oxidized organic compounds was detected.[18] During a 56-day test at a warmer temperature (24 °C), the concentration of acidic organic compounds reached a value between 1 and 2 mg/L during the investigation, and the relative abundance of the O_x-containing compounds (i.e., where $x > 2$) gradually increased during the experiment.

Our study was intended to provide a comprehensive characterization of the water-accommodated fractions contaminated by crude oil using a complementary approach to elucidate the composition of both polar and nonpolar water-accommodated organic compounds in a simulated freshwater–oil spill using negative-ion ESI Orbitrap-MS and positive-ion APPI FT-ICR-MS. Here, we review the application of negative-ion ESI Orbitrap-MS for the characterization of polar water-accommodated organic compounds, focusing on detailed molecular-level changes during the experiment.[19] The study presented here explored the detailed distribution of carbon number and double bond equivalent (DBE)[20] of components to analyze changes in the molecular-level composition of both polar and nonpolar water-accommodated organic compounds.

2. EXPERIMENTAL SECTION

2.1. Wave Tank Experiment. A 3 m × 2.1 m × 1.5 m ($L \times W \times H$) size mesoscale tank, situated in a well-vented indoor environment, was used to simulate oil spill conditions. A low-energy LED light with a wavelength range outside of ultraviolet was turned on only during operation (less than 2 h daily); these conditions were used to minimize/prevent photo-oxidative weathering. The detailed oil spill operating conditions have been reported previously.[21,22,19] Water was sampled directly from the North Saskatchewan River (NSR) (Alberta, Canada) with filtration (>0.45 μm) to remove particulates and undissolved material. To conduct the spill test, the NSR water was used to fill the mesoscale tank. When the water in the tank reached the designated temperature of 24 °C, the sediment content of the water was increased to 2000 mg/L by post hoc addition of 2.4 kg of river sediment obtained from the NSR flood plain, Alberta, Canada, and mixed for several minutes to distribute the sediment evenly throughout the test tank. A conventional crude oil (Mixed Sweet Blend, or MSW) obtained from a pipeline operator in Edmonton,

Alberta, was then introduced to the tank at a volume of 10 L. The properties of the crude oil used are listed in Table 1. All of the

Table 1. Properties of the Crude Oil[a,b]

parameter	value
saturates (wt %)	57.0
aromatics (wt %)	27.5
resins (wt %)	13.7
asphaltenes (wt %)	1.8
carbon (wt %)	86.2
hydrogen (wt %)	13.0
nitrogen (wt %)	0.03
sulfur (wt %)	0.7
oxygen (wt %)	<0.1
water (wt %)	0.1
density (g/mL) at 20 °C	0.8197
R^2	0.9999
viscosity (cSt) at 20 °C	4.7
R^2	0.9984

[a]Reproduced with permission from refs 18. Copyright 2020 John Wiley and Sons. [b]BP—boiling point.

properties of the crude oil sample were measured using the ASTM standard methods.[18] The simulated spill scenario was 56 days long, and 15 water samples were collected at regular intervals throughout the test. Further details can be found elsewhere.[19,21,22] Water samples from the tank were subjected to extraction and cleanup prior to MS analysis.

2.2. Sample Preparation. Solid-phase extraction (SPE) (Isolute ENV+, Biotage, Charlottesville, VA) was used, and the procedure followed existing protocols.[23] All SPE cartridges were labeled, rinsed, and conditioned with Milli-Q water, then aqueous samples (100 mL) were acidified with formic acid (pH < 2) and then passed through an SPE cartridge under vacuum. Cartridges were rinsed with 5 mL of Milli-Q water and then dried under gentle vacuum. The organic fraction retained in the column was eluted with 6 mL of methanol and dried under nitrogen. The organic fraction was reconstituted with 1 mL of acetonitrile/Milli-Q water (50:50) solution containing 0.1% ammonium hydroxide solution. All solvents used were liquid chromatography−mass spectrometry (LC−MS) grade products obtained from Fisher Scientific, Ottawa, ON, Canada, and used without any further purification.

2.3. Mass Spectrometry Analysis. *2.3.1. Negative-Ion ESI Orbitrap-MS Analysis.* Sample extracts were analyzed using an LTQ Orbitrap Elite mass spectrometer (Thermo Fisher Scientific, Waltham MA) at 240,000 resolution (measured at 400 m/z) operating in negative-ion ESI mode, and each mass spectra achieved a resolving power of 220,000 at m/z 400. Mass spectra were collected with a mass range of 100−600 m/z. In this work, we looked at molecular composition using both the Orbitrap-MS and FTICR-MS methods. The Orbitrap-MS mass scan range was from 100 to 600 m/z, while the FTICR-MS covers a wider range of 150−1000 m/z. The selected mass range of the Orbitrap-MS captures the mass region of the naphthenic acid mass envelope using negative-ion ESI typically found in historical samples. As this was our first analysis using APPI on these samples, a broader mass range was selected on the FTICR-MS to ensure full coverage was obtained from our unknown samples. The instrument conditions are set as follows: sheath gas flow rate 25 (arbitrary units); spray voltage 2.90 kV; auxiliary gas 5 (arbitrary units); S lens radio frequency level 67%; capillary temperature of 275 °C; heater temperature 50 °C; injection volume 5 μL. The infusion solvent was 50:50 acetonitrile:water with 0.1% NH$_4$OH at a flow rate of 200 μL/min.[24−28]

An oil sands process water-derived extract was used to calibrate the MS response to naphthenic acid fraction compounds (e.g., polar acidic organic compounds).[21−24] Oil sands process affected water from Fort McMurray, Alberta, Canada, which was collected in July
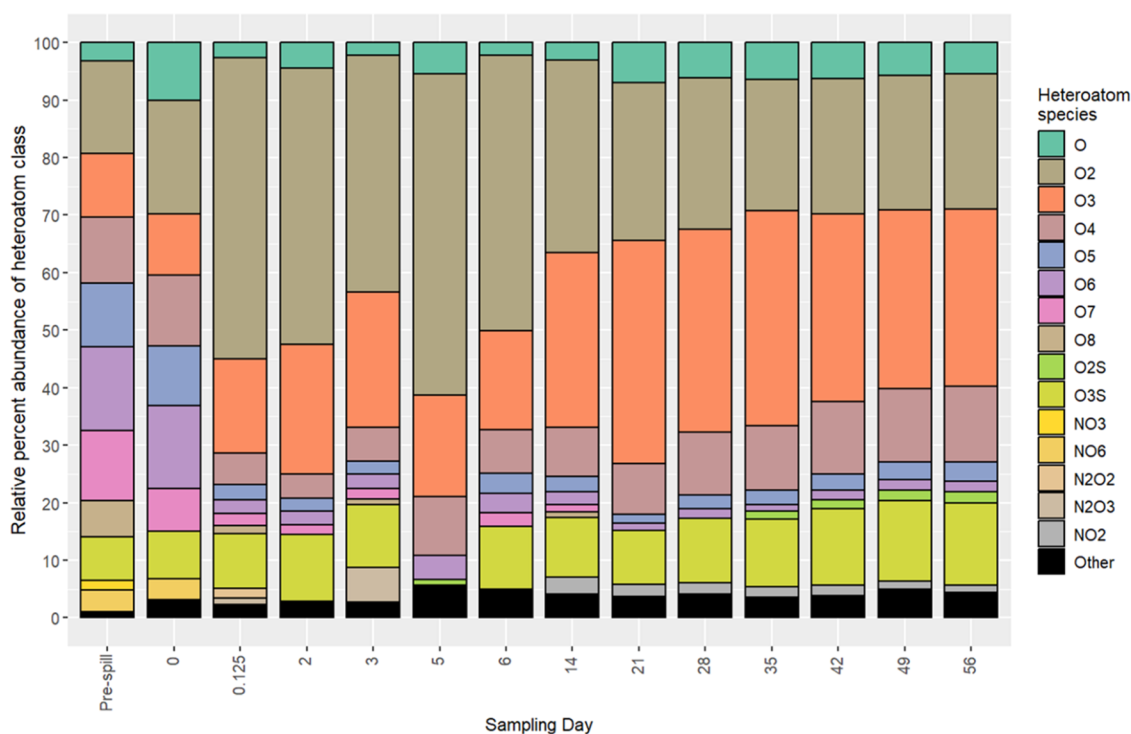
Figure 1. Relative abundance of heteroatom classes for the crude oil at different time points derived from the negative-ion ESI Orbitrap mass spectra. Note: others (black bars) indicate heteroatom classes with relative abundance of <1%. Reproduced with permission from ref 19. Copyright 2022 Elsevier.

2005. The concentration of the extract was measured using a calibration curve that links the concentration of the commercial standard to infrared (IR) peak absorbance.[29] The calibration solution containing the analytes of interest was prepared within the linear range of the calibration curve from 10 to 100 mg/L. Full details on the quantitation, quality control, and quality assurance steps are described elsewhere.[19] Sample extracts were diluted where necessary to bring sample extract concentrations into the linear detection range of the method. The method is considered semiquantitative; a lack of reference standards similarly limits other quantification methods.[30−32] An oil sand process-affected water-derived extract was used to calibrate the MS response to NAFCs (e.g., polar acidic organic compounds).[21−24]

Orbitrap mass spectra were initially processed for semiquantification and baseline subtraction using Xcalibur version 2.2 software (Thermo Fisher Scientific, Waltham MA). Formulas were assigned using Composer64 1.5.6 software (Sierra Analytics, Modesto CA). Composer64 formula assignment parameters were limited to compounds between 100 and 500 m/z and were restricted to assignments where mass error was <3 ppm.

2.3.2. Positive-Ion APPI 9.4 T FT-ICR-MS Analysis. Positive-ion APPI FT-ICR-MS was performed with a custom-built 9.4 FT-ICR mass spectrometer[33] equipped with a modular ICR data station and a 22 cm horizontal room temperature bore 9.4 T magnet (Oxford Corp., Oxney Mead, U.K.).[34] Mass spectra were phased-corrected[35] in absorption mode, "walking"[36] calibrated based on internal homologous series, acquired with Predator data station[38] and element PetroOrg software.[37] To identify homologous series for each heteroatom class, a Kendrick mass defect analysis[38,39] was performed to verify the accuracy of the elemental composition assignments (i.e., species that have the same $C_cH_hN_nO_oS_s$ composition but differ only in the extent of alkylation).[39,40] For each APPI FT-ICR mass spectrum, more than 20,000 unique elemental compositions were assigned at <100 ppb RMS mass error, and the number of peak assignments and mass measurement accuracy of all molecular species identified are listed in the Supporting Information (SI) for the negative-ion ESI Orbitrap-MS (S1) and the positive-ion APPI FT-ICR-MS (S2). To

rapidly visualize the tens of thousands of individual species APPI-FT-ICR-MS data, carbon number (#C) versus DBE and heteroatom class distribution profiles were created. The following elemental compositions were assigned: H unlimited, 0 < C < 100, 0 < O < 12, 0 < N < 2, 0 < S < 2, 0 < DBE < 30. Only chemical formulas with appropriate ^{13}C peaks for hydrocarbons and ^{34}S peaks for sulfur assignments m/z in the 150 < m/z < 1000 range were taken into consideration.[40]

2.4. Data Analysis. All formula data from all samples, as assigned by Composer64 or PetroOrg, were imported into R version 4.0.3 software where plots were prepared with ggplot2, a component of the tidyverse package.[41]

3. RESULTS AND DISCUSSION

3.1. Heteroatom Class Species Characterized by ESI Orbitrap-MS and APPI FT-ICR-MS. To assess a broad selection of compound classes and polarities, data from both negative-ion ESI Orbitrap-MS and positive-ion APPI FT-ICR-MS were initially evaluated using bar plots of percent spectral heteroatom abundance. Figure 1 shows the class analysis diagram for the major heteroatoms obtained from negative-ion ESI Orbitrap-MS. Prior to the spill, O_x (x = 1−8) heteroatom classes were the most prevalent in the water. As illustrated by the formula diversity in Figure 1, natural organic matter (NOM) detected in negative-ion ESI in river water (pre-spill) included mostly O_x compounds, with <15% of formulas represented by other single heteroatom classes. As oil was introduced to the spill tank, the molecular diversity shifted rapidly, where O_2-containing formulas became dominant across sample spectra within 3 h (Day 0.125), reaching a maximum relative abundance after 5 days. Thereafter, O_3, O_4, and O_5 compounds gradually increased in relative abundance, especially for the O_3 and O_4 classes, whereas the O_2 compounds gradually decreased. A trend in the data was apparent where more-oxidized formulas (e.g., O_3, O_4, and O_5)
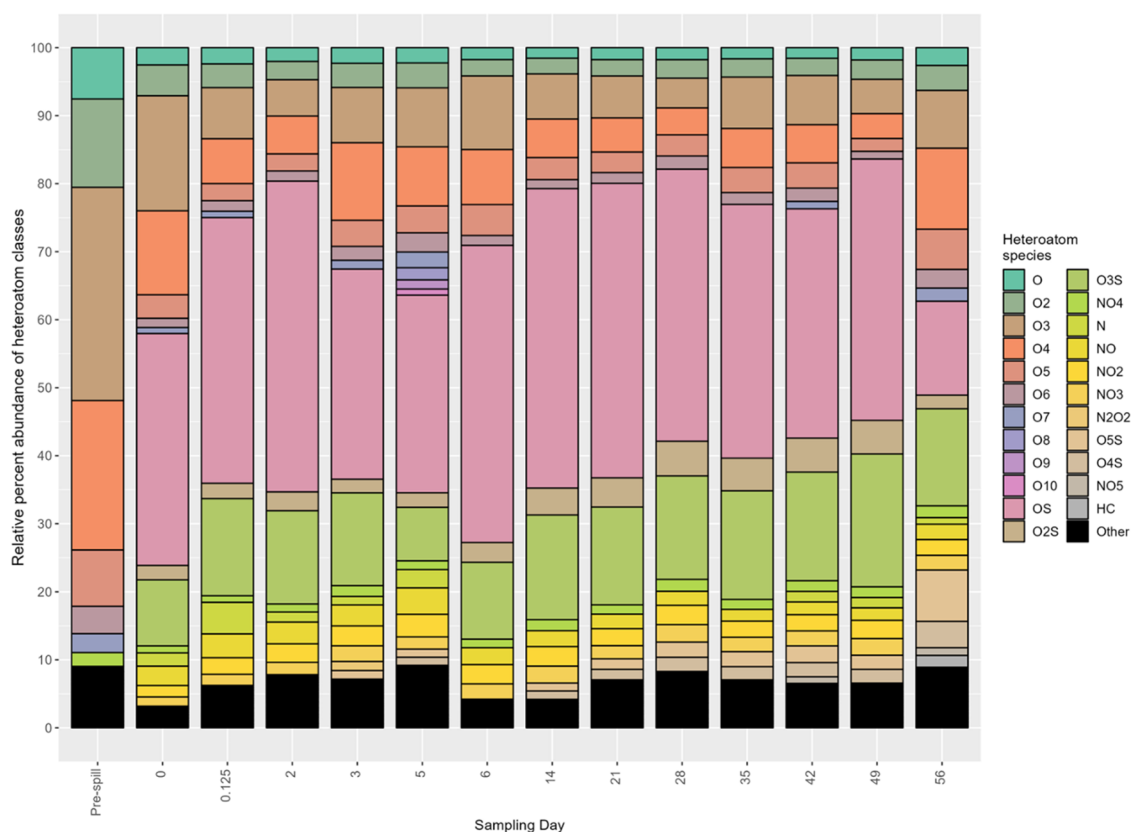
Figure 2. Relative abundance of heteroatom classes for the crude oil at different time points derived from the positive-ion APPI FT-ICR mass spectra. "Other" (black bars) indicate heteroatom classes with relative abundance of <1%.

emerged chronologically relative to the degree of oxygen incorporation, which may suggest sequential oxidation of petroleum-derived mixture components. From Day 0.125 (i.e., 3 h) to Day 6, the relative abundances of the O_2, O_3, and O_4 classes increased (in the order of $O_2 > O_3 > O_4$), consistent with earlier work.[42] From Days 21 to 56, the O_2 class appeared to have reached a steady state, whereas there was a noticeable increase in the relative abundances of the O_3 and O_4 compounds over the same period. Oxygen-rich O_x ($x \geq 3$) compounds are presumably intermediates produced through transformation of the O_2 class.[43] In addition, the SO_x classes increased in relative abundance while the relative abundance of the NO_x species increased slightly with the duration of the spill, which suggests that other nitrogen and sulfur compounds may convert into these species, consistent with previous findings.[44,45] It is worth noting that on Day 5, there was no presence of the SO_3 species. These compounds may be more affected by transformation than other classes. The relative abundance of SO_3 classes increased from day 6 to Day 56, which could be due to the relatively rapid transformation of other sulfur-containing classes, such as SO_4.

To better characterize nonpolar aromatic compounds in oil-affected river water from the oil spill test, positive-ion APPI was used to examine compounds and classes that might otherwise be missed by ESI. The same sample extracts described above were subsequently characterized using positive-ion APPI FT-ICR-MS. Like negative-ion ESI, the heteroatom content of river water was dominated at the outset by oxygen-containing compounds. Over time, the composition and relative abundances of sulfur (SO_x) and nitrogen (NO_x) compounds varied compared to those of background river

water DOM (pre-spill). No discernible trend could be observed for the relative abundances of the SO_x and NO_x species over time. Greater diversity of sulfur-containing classes with high relative abundances of the SO and SO_3 classes occurred over time, which may be a result of oxidation or breakdown of other sulfur-containing species. The crude oil used in this study contains S (0.7 wt %). The increase in the relative abundance and diversity of SO_x species observed over time during the spill test may indicate that oxidation of the S class was at least partly responsible for these changes. It has been suggested that the reason for the existence of the SO_x classes is probably the oxidation of the S species.[45,46] Positive-ion mode is typically used to identify sulfur compounds. However, since there was no S detected, it is likely that their further oxidation to the SO_x classes in the samples may have reduced them to a nondetectable level, which could have provided information at the molecular level on the formation of the SO_x species from the S class. To better characterize nonpolar aromatic compounds in crude oil, positive-ion APPI was used. Compounds and classes that might otherwise be unresolved by the Orbitrap-MS were studied. The high prevalence of peak coalescence behavior limits the ability of the Orbitrap MS to resolve closely spaced mass spectral peaks (<3.4 mDa) with ion number targets required for complex mixture analysis (i.e., AGC > 5E5).[47] This results in multiple ionized species coalescing inside the Orbitrap detection cell and an incorrect elemental composition assignment. Therefore, we applied APPI FT-ICR-MS, which routinely achieves resolving powers in excess of 1,000,000 at m/z 400,[48] sufficient to identify isobaric species that differ in mass by roughly the
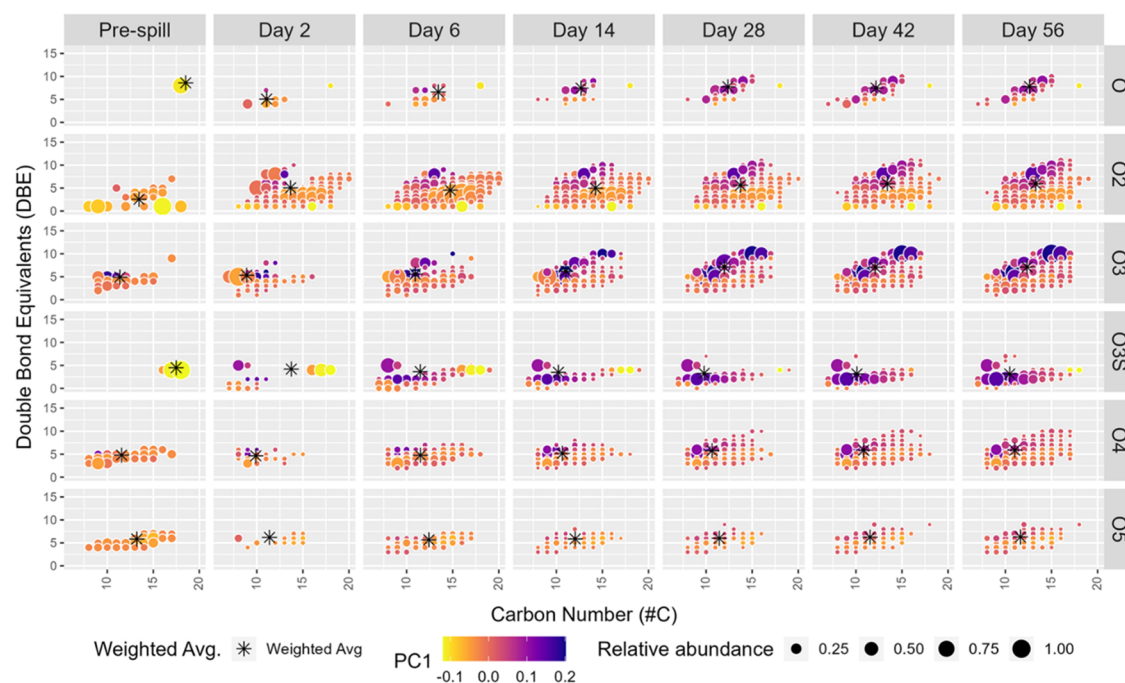
Figure 3. Distribution of the relative abundance average of #C versus DBE of major heteroatom compounds observed by negative-ion ESI Orbitrap-MS in selected chronological samples. Formulas detected by the Orbitrap-MS used in principal component analysis are color-coded according to their associated scores along PC1.
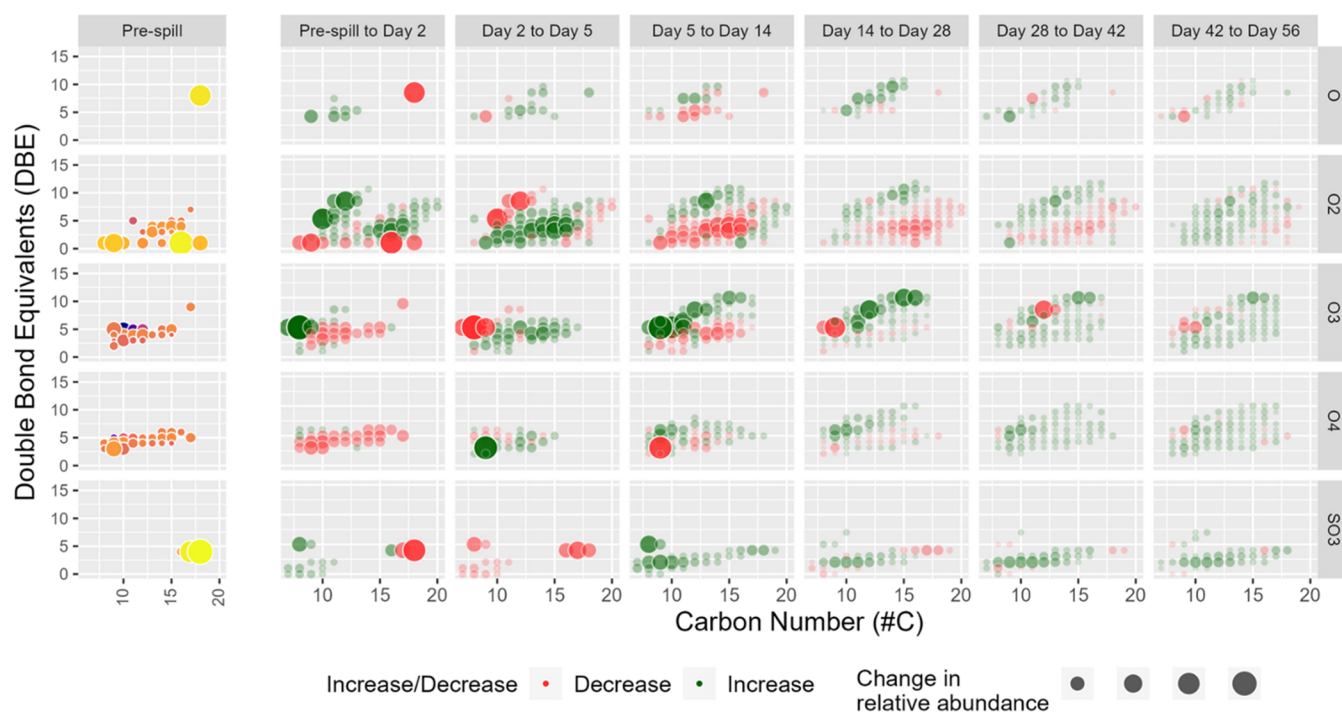
Figure 4. Chronological #C and DBE plots of the increases and decreases of formulas from major heteroatom classes between selected time points observed by negative-ion ESI Orbitrap-MS. Red indicates a lower relative abundance of a particular formula (i.e., a net decrease across time), and green indicates a net increase across time. The relative ion abundance in the spectra is shown by the magnitude of the circles.

mass of an electron. Figure 2 shows heteroatom class distribution plots for the APPI FT-ICR-MS mass spectra.

As observed by negative-ion ESI Orbitrap-MS, oxygen-containing compounds dominated river water early in the spill. However, further evaluation by APPI FT-ICR-MS highlights the limitation of negative-ion ESI Orbitrap-MS for oil spill characterization. Importantly, this study highlights the

limitations of simply using negative-ion electrospray ionization for weathered oil studies, where the resolving power and resolution achieved by Orbitrap-MS are ineffective in accurately evaluating weathered oil oxygen-rich compounds. The plot of the fraction of total signal assignable over time detected by the negative-ion ESI Orbitrap-MS and positive-ion APPI FT-ICR-MS is shown in Figure S1. Quantitation of total
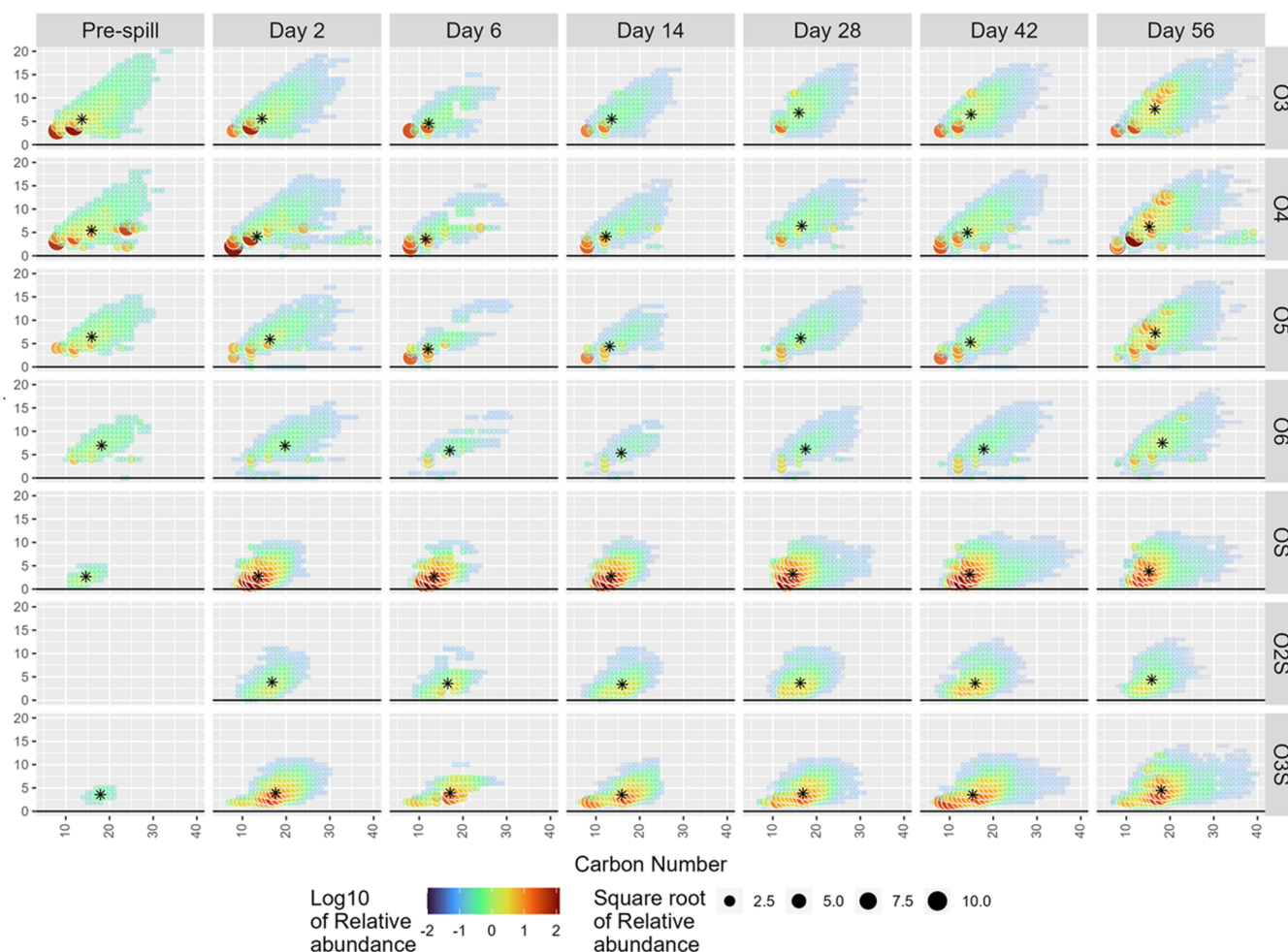
Figure 5. Distribution of the relative abundance of #C versus DBE of major heteroatom compounds observed by positive-ion APPI FT-ICR-MS in selected chronological samples. The relative abundance-weighted average is indicated by the asterisk (*).

NAFCs, the water-accommodated fraction, and polar acidic compounds (PACs) was previously reported.[19]

3.2. Visualizations of Distribution of Carbon Number (#C) and DBE from ESI Orbitrap-MS and APPI FT-ICR-MS. To gain insights into the transformation of water-soluble organic compounds and enhance our understanding of the fate and behavior of the oil spill in freshwater at a molecular level, we examined the changes in the distribution of carbon number and DBE of components. From selected samples, #C versus DBE plots of major heteroatom classes were prepared and reported with weighted average #C and DBE to compare chronological distributions of formulas. The weighted average DBE and carbon number values of all of the detected ions were calculated for each formula to reduce the data to a representative value for each formula by adding together the product of the mass-to-charge (m/z) ratio and the relative abundance of each detected ion associated with the formulas and dividing by the total relative abundance of all of the detected ions for each time point. As illustrated in Figure 3 (only shows ESI Orbitrap), and formula diversity of all heteroatom classes increased over time, For example, the number of O_2 compounds detected increased rapidly in relative abundance by Day 2, reaching a maximum weighted average #C by Day 6, where species detected thereafter tend to decrease in relative abundance of #C. Notably, the DBE of O_2 species increased throughout, demonstrating that the most-

unsaturated O_2 species tend to persist under these conditions. This observation suggests that the saturated O_2-containing compounds preferentially degrade compared to unsaturated O_2 species. This finding is consistent with the reported higher rate of biodegradation associated with lower DBE distributions.[49−51] In comparison, O_3, O_4, and O_5 compounds were more abundant from Day 6 onward, where the relative abundance of #C and DBE increased over the rest of the experiment. The apparent chronological emergence of O_x species with an increasing value of x suggests that these compounds may be sequentially related (e.g., that O_3 are emerging as products of O_2 oxidation, O_4 of O_3− oxidation, etc.).[52] Compounds that have comparable weighted average #C values but relatively more oxygen (i.e., O_x where $x > 2$) might be expected to be more water-soluble than those O_2 compounds that emerge first in the simulated spill conditions. In comparison, SO_3 species may partition slowly from the oil or could emerge over time as byproducts of oxidation of sulfur-containing hydrocarbons. The sequential increase in the relative abundance of the O_x (where $x \geq 3$) compounds provides additional evidence that oxidation occurs in series and that once oxidized, these compounds likely become more susceptible to further oxidation.

To show which mixture components more clearly were increasing or decreasing during the spill, base-peak-normalized relative abundance plots comparing negative-ESI spectra by #C
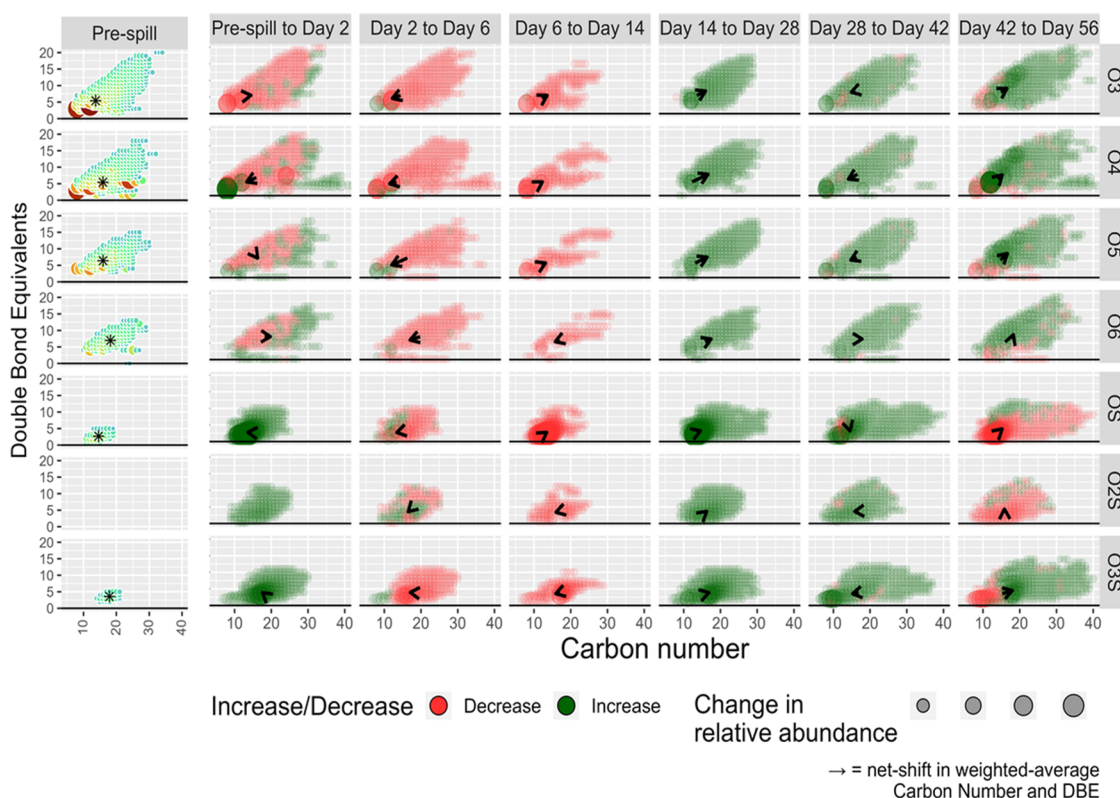
Figure 6. Distribution of chronological #C and DBE showing the increases and decreases of formulas from major heteroatom classes between selected time points observed by positive-ion APPI FT-ICR-MS. Red indicates a lower relative abundance of a particular formula (i.e., a net decrease across time), and green indicates a net increase across time. The relative ion abundance in the spectra is shown by the magnitude of the circles. The arrows show the net change in the weighted average carbon number and DBE. The < shows a decrease in weighted average, and the > shows an increase in weighted average.

versus DBE were prepared, as illustrated in Figure 4. These plots show net changes in the base-peak-normalized relative abundance of particular formulas.[53] The O_2 and O_3 species initially increased in relative abundance from pre-spill to Day 2 in Figure 4, whereas other compound classes emerged later. From Day 6 to Day 56, decreases in O_2 species were most prominent among higher-#C (C > 13) formulas, whereas coinciding increases in O_2 species were concentrated among lower-#C species (#C < 12) with higher DBE (>4). These combined observations are consistent with biodegradation. Despite specific decreases in particular formula abundance, the whole of the O_2 species gradually increased in diversity and molecular complexity (i.e., increasing DBE) from Day 2 to Day 56, with a greater number of identified formulas present by Day 55 compared to any prior sample. Simultaneously, O_3 and O_4 compounds tended to increase in relative abundance throughout the duration of the simulated spill, where increases in relative abundances of these formula classes were generally among low-#C formulas with elevated DBE. In the absence of advanced oxidation treatments, highly unsaturated compounds tend to be more recalcitrant to biodegradation or bio-uptake.[54−56]

Degradation of components may also occur via other pathways. For example, abiotic sorption may be possible, as there was river sediment present during the simulated oil spill. However, sorption of NAs in well-mixed systems is reported to occur rapidly.[57,58] As the rates of degradation of the oil appear to be relatively slow, occurring over days, sorption to sediments may not be dominant for the polar acidic organic compounds over the 56-day period of the oil spill. In addition,

previous studies evaluating sorption of model compounds onto soils occurred in the absence of petroleum.[58,59] The extent to which nonpolar compounds preferentially sorb onto sediments and occupy binding sites that would otherwise be available to polar organic compounds is not known.

To more closely examine the distributions of the major compound classes derived from the positive-ion APPI FT-ICR mass spectra, a plot of the relative abundances of #C and DBE was prepared (Figure 5). A clear trend in the transformation of oxygen-containing compounds during the simulated spill was observed. Initially, the pre-spill sample contained substantial amounts of naturally occurring oxygen-containing components from the sediment (O_3, O_4, O_5, and O_6). The oxygen-containing classes found in the river water sample were found in significant relative abundances, which may have biogenic origins. By Day 2, the abundance of these compounds had noticeably decreased, and this trend continued until Day 14. From Day 28 onward, the relative abundances of these compounds started to increase again in different regions of the #C and DBE plots. By Day 56, more unsaturated and high carbon number species of oxygen-containing compounds were prevalent. In summary, the data revealed a dynamic process involving the transformation of oxygen-containing compounds. The initial decrease in relative abundance followed by an increase in the relative abundance of the same components may suggest a multiphasic behavior where the compounds partition selectively between the aqueous and organic phases. The transformations observed may also be due to time-dependent pathways resulting in either the degradation or

formation of components, a topic that warrants further investigation.

There were also trends related to sulfur-containing compounds (SO, SO₂, and SO₃) during the experiment. The sulfur-containing compounds were present in the pre-spill at a very low relative abundance. By Day 2, the relative abundances of these sulfur-containing compounds had increased substantially, after which high levels were maintained throughout the spill. The relative abundance of the SO_3-containing compounds showed a gradual increase relative to that of the SO and SO_2 compounds. This observation may suggest that over time, there was a shift in the composition of sulfur-containing compounds toward a higher proportion of SO_3-containing species.

To further investigate temporal trends in the molecular distribution of the heteroatom classes, from positive-ion APPI FT-ICR-MS mass spectra, a net-change visualization of formulas according to #C and DBE of formulas is given in Figure 6. As illustrated in Figure 6, there were substantial amounts of naturally occurring dissolved organic matter O_x ($x \geq 3$) species present in the water pre-spill. Most of the O_x-containing compounds observed on Day 2 decreased substantially by Day 6 to 14. The initial decrease in the relative abundances of the O_x-containing compounds may be due to the partitioning of oxygen-containing compounds to natural organic matter (DOM) in the alluvial sediment over this period. The relative abundances of O_x-containing compounds gradually increased after Day 14, and components were generally more unsaturated with higher #C by Day 56 compared to the pre-spill conditions.

The relative abundances of sulfur-containing compounds increased gradually from Day 2 onward. Their abundances did not change appreciably up to Day 14, but increased substantially from Day 14 onward, likely because of further weathering. The number of sulfur-containing compound classes (i.e., SO, SO₂, and SO₃) generally increased throughout the simulated spill (except for the slight net-loss from Day 2 to 6 and Day 6 to 14). In contrast, the relative abundances of higher-molecular-weight SO_x-containing compounds increased during the experiment. Increases in the SO_3 compound class were more prominent than those in the SO-containing compounds throughout the experiment. Figure 6 highlights a trend observed within the sulfur-containing classes (SO and SO₃), where higher #C and DBE compounds persisted. The latter may thus be relatively stable transformation products from the weathering of the oil in the simulated spill.

The molecular-level characterizations above demonstrate the utility of complementary characterizations for a comprehensive description of oil spill chemistry. The negative-ion ESI Orbitrap-MS was sensitive to a range of low-molecular-weight polar compounds, where the emergence of the O_x species with the passage of time describes an oxidizing trend. Furthermore, positive-ion APPI FT-ICR-MS revealed additional compounds with higher #C and DBE values that were not observed using negative-ion ESI Orbitrap-MS. The negative-ion ESI analysis showed a dominance of the O_x classes (particularly the O_2 species) compared to those identified using positive-ion APPI. The O_2 acidic classes may be oxidized to species that are more recalcitrant over time. Polar organics in the freshwater spill can therefore progressively become oxygen-rich over time, and the highly unsaturated and/or conjugated species were the most stable in this system. A recent study examined NAs affected by diluted bitumen (DB) in a spill tank using high-resolution negative-ion ESI Orbitrap-MS. The researchers observed a decrease in the relative abundance of O_2 species and a corresponding increase in the relative abundance of O_3 species over time.[22] The carbon number and DBE distribution for the O_2 species can provide further evidence of biodegradation. The O_x species with higher DBE distributions were found to be more stable in the system over time in this study. Similar findings were reported in a previous study by Monaghan et al.,[22] where O_3 compounds with higher DBE were also observed to be more persistent in the system over time. These consistent observations across different studies indicate that the shifts in relative abundance and DBE distribution data for the O_x species are likely attributed to oxidative mechanisms facilitated by diverse microbial populations present in the systems. The apparent enrichment of oxygen-rich species over the duration of the spill, specifically higher abundances of O_3- and O_4-containing species, is a possible indicator of biodegradation.[60]

For the positive-ion FT-ICR-MS APPI studies, an increased relative abundance of the higher-molecular-weight SO_x coincided with a decrease in the relative abundances of the lower-molecular-weight species. This observation is of environmental importance as SO_x-containing compounds are implicated as principal toxicants in aquatic systems.[61] Lower-molecular-weight species may have progressively diminished through volatilization or degradation. Selective loss of lower mass compounds led to the emergence of the heavier and more unsaturated analogues, for which the latter are likely more recalcitrant. Like results for negative-ion ESI Orbitrap-MS data, an increase in the relative abundances was observed for the more unsaturated and high-#C species over time.

4. CONCLUSIONS

Conventional crude oil was used to simulate a freshwater–oil spill and was characterized by both negative-ion Orbitrap-MS and positive-ion APPI-FT-ICR-MS. Detailed molecular-level characterization of chemical components improved our understanding of factors affecting the environmental transformation and fate of the spilled oil. According to negative-ion ESI Orbitrap-MS data, oxygen-containing species were the primary compounds observed in the water samples. Changes in the distribution of O_x-containing components occurred with increasing levels of oxygen incorporation with the duration of the spill. Thus, compounds with increasing degrees of oxidation (e.g., O_2, O_3, and O_4) tended to emerge later in the spill. The relative abundance of the most-unsaturated compounds increased with the duration of the spill, consistent with recalcitrance of such compounds to biodegradation. On the other hand, positive-ion APPI FT-ICR-MS analysis provided complementary insights for an improved understanding of the weathering of oil spills in freshwater. APPI data demonstrated an increased abundance of higher-molecular-weight SO_x-class compounds with time, and reinforced observations from the ESI Orbitrap analysis, mainly the increase of unsaturated and high-molecular-weight compounds in later days of the simulated spill. The use of both analytical techniques on the same sample set leverages the benefits of both, capturing lower-molecular-weights with Orbitrap, and larger, more complex molecules with FT-ICR-MS. There are many complex weathering and transformation mechanisms occurring after a spill, and this work has provided a more thorough understanding of the oxidation of hydrocarbons in a freshwater system.

■ ASSOCIATED CONTENT

ⓈⒾ Supporting Information

The Supporting Information is available free of charge at https://pubs.acs.org/doi/10.1021/acs.energyfuels.3c04994.

Number of peak assignments and mass measurement accuracy of all molecular species identified by the negative-ion ESI Orbitrap mass spectrometry (Table S1); number of peak assignments and root-mean-square error (RMS) of all molecular species identified by the positive-ion atmospheric pressure photoionization Fourier transform ion cyclotron resonance (Table S2); and changes in the total relative abundance of the heteroatom compounds over time detected by negative-ion ESI Orbitrap-MS and positive-ion APPI FT-ICR-MS (Figure S1) (PDF)

■ AUTHOR INFORMATION

Corresponding Author

Dena W. McMartin − *Department of Geography and Environment, University of Lethbridge, Lethbridge, Alberta T1K 3M4, Canada; Department of Civil, Geological and Environmental Engineering, 57 Campus Drive, University of Saskatchewan, Saskatoon, Saskatchewan S7N 5A9, Canada;* ⓞ orcid.org/0000-0002-0824-0565; Email: dena.mcmartin@uleth.ca

Authors

Chukwuemeka Ajaero − *Environment and Climate Change Canada, Watershed Hydrology and Ecology Research Division, National Hydrology Research Center, Saskatoon, Saskatchewan S7N 3H5, Canada; Department of Geography and Environment, University of Lethbridge, Lethbridge, Alberta T1K 3M4, Canada*

Ian Vander Meulen − *Environment and Climate Change Canada, Watershed Hydrology and Ecology Research Division, National Hydrology Research Center, Saskatoon, Saskatchewan S7N 3H5, Canada; Department of Civil, Geological and Environmental Engineering, 57 Campus Drive, University of Saskatchewan, Saskatoon, Saskatchewan S7N 5A9, Canada*

Nicole E. Heshka − *CanmetENERGY Devon, Natural Resources Canada, Devon, Alberta T9G 1A8, Canada;* ⓞ orcid.org/0000-0002-8188-5888

Qin Xin − *CanmetENERGY Devon, Natural Resources Canada, Devon, Alberta T9G 1A8, Canada*

Kerry M. Peru − *Environment and Climate Change Canada, Watershed Hydrology and Ecology Research Division, National Hydrology Research Center, Saskatoon, Saskatchewan S7N 3H5, Canada*

Huan Chen − *National High Field Magnet Laboratory, Florida State University, Tallahassee, Florida 32306, United States;* ⓞ orcid.org/0000-0002-6032-6569

Amy M. McKenna − *National High Field Magnet Laboratory, Florida State University, Tallahassee, Florida 32306, United States; Soil and Crop Sciences, Colorado State University, Fort Collins, Colorado 80523, United States;* ⓞ orcid.org/0000-0001-7213-521X

Kiaura Reed − *Department of Biology, College of Science and Technology, Florida Agricultural and Mechanical University, Tallahassee, Florida 32307, United States*

John V. Headley − *Environment and Climate Change Canada, Watershed Hydrology and Ecology Research Division, National Hydrology Research Center, Saskatoon, Saskatchewan S7N 3H5, Canada*

Complete contact information is available at:
https://pubs.acs.org/10.1021/acs.energyfuels.3c04994

Notes

The authors declare no competing financial interest.

■ REFERENCES

(1) Government of Canada, C. E. R. CER − Crude Oil Pipeline Transportation System. https://www.cer-rec.gc.ca/en/data-analysis/facilities-we-regulate/canadas-pipeline-system/2021/crude-oil-pipeline-transportation-system.html#:~:text=Most%20of%20Canada%27s%20crude%20oil,as%20shown%20in%20Figure%2010.&text=Description%3A%20The%20pie%20chart%20shows,and%207.8%25%20by%20marine%20tankerhttps://www.cer-rec.gc.ca/en/data-analysis/facilities-we-regulate/canadas-pipeline-system/2021/crude-oil-pipeline-transportation-system.html#:~:text=Most%20of%20Canada%27s%20crude%20oil,as%20shown%20in%20Figure%2010.&text=Description%3A%20The%20pie%20chart%20shows,and%207.8%25%20by%20marine%20tanker (accessedJun 20, 2023).

(2) Daisy, N. S.; Hafezi, M. H.; Liu, L.; Lee, K. A Comprehensive Review of Canadian Marine Oil Spill Response System through the Lens of Decanting Regulations and Practices. *J. Mar. Sci. Eng.* **2022**, *10* (9), No. 1310, DOI: 10.3390/jmse10091310.

(3) Wang, Z.; Stout, S. A.; Fingas, M. Forensic Fingerprinting of Biomarkers for Oil Spill Characterization and Source Identification. *Environ. Forensics* **2006**, *7* (2), 105−146.

(4) Hegazi, A. H.; Fathalla, E. M.; Panda, S. K.; Schrader, W.; Andersson, J. T. High-Molecular Weight Sulfur-Containing Aromatics Refractory to Weathering as Determined by Fourier Transform Ion Cyclotron Resonance Mass Spectrometry. *Chemosphere* **2012**, *89* (3), 205−212.

(5) Wang, C.; Chen, B.; Zhang, B.; He, S.; Zhao, M. Fingerprint and Weathering Characteristics of Crude Oils after Dalian Oil Spill, China. *Mar. Pollut. Bull.* **2013**, *71* (1), 64−68.

(6) Faksness, L.-G.; Daling, P.; Altin, D.; Dolva, H.; Fosbæk, B.; Bergstrøm, R. Relative Bioavailability and Toxicity of Fuel Oils Leaking from World War II Shipwrecks. *Mar. Pollut. Bull.* **2015**, *94* (1), 123−130.

(7) Idowu, O.; Semple, K. T.; Ramadass, K.; O'Connor, W.; Hansbro, P.; Thavamani, P. Beyond the Obvious: Environmental Health Implications of Polar Polycyclic Aromatic Hydrocarbons. *Environ. Int.* **2019**, *123*, 543−557.

(8) Bejarano, A. C.; Michel, J. Oil Spills and Their Impacts on Sand Beach Invertebrate Communities: A Literature Review. *Environ. Pollut.* **2016**, *218*, 709−722.

(9) McKenna, A. M.; Nelson, R. K.; Reddy, C. M.; Savory, J. J.; Kaiser, N. K.; Fitzsimmons, J. E.; Marshall, A. G.; Rodgers, R. P. Expansion of the Analytical Window for Oil Spill Characterization by Ultrahigh Resolution Mass Spectrometry: Beyond Gas Chromatography. *Environ. Sci. Technol.* **2013**, *47* (13), 7530−7539.

(10) Huba, A. K.; Gardinali, P. R. Characterization of a Crude Oil Weathering Series by Ultrahigh-Resolution Mass Spectrometry Using Multiple Ionization Modes. *Sci. Total Environ.* **2016**, *563−564*, 600−610.

(11) Huba, A. K.; Huba, K.; Gardinali, P. R. Understanding the Atmospheric Pressure Ionization of Petroleum Components: The Effects of Size, Structure, and Presence of Heteroatoms. *Sci. Total Environ.* **2016**, *568*, 1018−1025.

(12) Koolen, H. H. F.; Swarthout, R. F.; Nelson, R. K.; Chen, H.; Krajewski, L. C.; Aeppli, C.; McKenna, A. M.; Rodgers, R. P.; Reddy, C. M. Unprecedented Insights into the Chemical Complexity of Coal Tar from Comprehensive Two-Dimensional Gas Chromatography Mass Spectrometry and Direct Infusion Fourier Transform Ion Cyclotron Resonance Mass Spectrometry. *Energy Fuels* **2015**, *29* (2), 641−648.

(13) Ajaero, C.; Headley, J. V.; Peru, K. M.; McMartin, D. W.; Barrow, M. P. Forensic Studies of Naphthenic Acids Fraction Compounds in Oil Sands Environmental Samples and Crude Oil. In *Standard Handbook Oil Spill Environmental Forensics*, 2nd ed.; Stout, S. A.; Wang, Z., Eds.; Academic Press: Boston, 2016; pp 343−397.

(14) Headley, J. V.; Peru, K. M.; Barrow, M. P. Advances in Mass Spectrometric Characterization of Naphthenic Acids Fraction Compounds in Oil Sands Environmental Samples and Crude Oil—A Review. *Mass Spectrom. Rev.* **2016**, *35* (2), 311−328.

(15) Meulen, I. J. V.; Downham, R.; Alostad, L.; Peru, K.; McMartin, D.; Barrow, M.; Headley, J. 3 Advances in Fourier Transform Mass Spectrometry Forensic Tools for Naphthenic Acid Fraction Compounds in Oil Sand Environmental Samples and Crude Oil. In *The Chemistry of Oil and Petroleum Products*; De Gruyter, 2022.

(16) Lababidi, S.; Schrader, W. Online Normal-Phase High-Performance Liquid Chromatography/Fourier Transform Ion Cyclotron Resonance Mass Spectrometry: Effects of Different Ionization Methods on the Characterization of Highly Complex Crude Oil Mixtures. *Rapid Commun. Mass Spectrom.* **2014**, *28* (12), 1345−1352.

(17) Kondyli, A.; Schrader, W. Evaluation of the Combination of Different Atmospheric Pressure Ionization Sources for the Analysis of Extremely Complex Mixtures. *Rapid Commun. Mass Spectrom.* **2020**, *34* (8), No. e8676.

(18) Lara-Jacobo, L. R.; Gauthier, C.; Xin, Q.; Dupont, F.; Couture, P.; Triffault-Bouchet, G.; Dettman, H. D.; Langlois, V. S. Fate and Fathead Minnow Embryotoxicity of Weathering Crude Oil in a Pilot-Scale Spill Tank. *Environ. Toxicol. Chem.* **2021**, *40* (1), 127−138.

(19) Heshka, N. E.; Peru, K. M.; Xin, Q.; Dettman, H. D.; Headley, J. V. High Resolution Orbitrap Mass Spectrometry Analysis of Oxidized Hydrocarbons Found in Freshwater Following a Simulated Spill of Crude Oil. *Chemosphere* **2022**, *292*, No. 133415.

(20) McLafferty, F. W.; Tureček, F. *Interpretation of Mass Spectra*, 4th ed.; University Science Books: Mill Valley, Calif, 1993.

(21) Xin, Q.; Saborimanesh, N.; Greer, C. W.; Farooqi, H.; Dettman, H. D. The Effect of Temperature on Hydrocarbon Profiles and the Microbial Community Composition in North Saskatchewan River Water during Mesoscale Tank Tests of Diluted Bitumen Spills. *Sci. Total Environ.* **2023**, *859*, No. 160161.

(22) Monaghan, J.; Xin, Q.; Aplin, R.; Jaeger, A.; Heshka, N. E.; Hounjet, L. J.; Gill, C. G.; Krogh, E. T. Aqueous Naphthenic Acids and Polycyclic Aromatic Hydrocarbons in a Meso-Scale Spill Tank Affected by Diluted Bitumen Analyzed Directly by Membrane Introduction Mass Spectrometry. *J. Hazard. Mater.* **2022**, *440*, No. 129798.

(23) Headley, J. V.; Peru, K. M.; McMartin, D. W.; Winkler, M. Determination of Dissolved Naphthenic Acids in Natural Waters by Using Negative-Ion Electrospray Mass Spectrometry. *J. AOAC Int.* **2002**, *85* (1), 182−187.

(24) Bauer, A. E.; Frank, R. A.; Headley, J. V.; Peru, K. M.; Hewitt, L. M.; Dixon, D. G. Enhanced Characterization of Oil Sands Acid-Extractable Organics Fractions Using Electrospray Ionization−High-Resolution Mass Spectrometry and Synchronous Fluorescence Spectroscopy. *Environ. Toxicol. Chem.* **2015**, *34* (5), 1001−1008.

(25) Meulen, I. J. V.; Klemish, J. L.; Peru, K. M.; Chen, D. D. Y.; Pyle, G. G.; Headley, J. V. Molecular Profiles of Naphthenic Acid Fraction Compounds from Mine Lease Wetlands in the Athabasca Oil Sands Region. *Chemosphere* **2021**, *272*, No. 129892, DOI: 10.1016/j.chemosphere.2021.129892.

(26) Headley, J. V.; Peru, K. M.; Fahlman, B.; Colodey, A.; McMartin, D. W. Selective Solvent Extraction and Characterization of the Acid Extractable Fraction of Athabasca Oils Sands Process Waters by Orbitrap Mass Spectrometry. *Int. J. Mass Spectrom.* **2013**, *345−347*, 104−108.

(27) Headley, J. V.; Peru, K. M.; Janfada, A.; Fahlman, B.; Gu, C.; Hassan, S. Characterization of Oil Sands Acids in Plant Tissue Using Orbitrap Ultra-High Resolution Mass Spectrometry with Electrospray Ionization. *Rapid Commun. Mass Spectrom.* **2011**, *25* (3), 459−462.

(28) Martin, J. W.; Han, X.; Peru, K. M.; Headley, J. V. Comparison of High- and Low-Resolution Electrospray Ionization Mass Spectrometry for the Analysis of Naphthenic Acid Mixtures in Oil Sands Process Water. *Rapid Commun. Mass Spectrom.* **2008**, *22* (12), 1919−1924.

(29) Ripmeester, M. J.; Duford, D. A. Method for Routine "Naphthenic Acids Fraction Compounds" Determination in Oil Sands Process-Affected Water by Liquid-Liquid Extraction in Dichloromethane and Fourier-Transform Infrared Spectroscopy. *Chemosphere* **2019**, *233*, 687−696.

(30) Ajaero, C.; Peru, K. M.; Simair, M.; Friesen, V.; O'Sullivan, G.; Hughes, S. A.; McMartin, D. W.; Headley, J. V. Fate and Behavior of Oil Sands Naphthenic Acids in a Pilot-Scale Treatment Wetland as Characterized by Negative-Ion Electrospray Ionization Orbitrap Mass Spectrometry. *Sci. Total Environ.* **2018**, *631−632*, 829−839.

(31) Duncan, K. D.; Letourneau, D. R.; Vandergrift, G. W.; Jobst, K.; Reiner, E.; Gill, C. G.; Krogh, E. T. A Semi-Quantitative Approach for the Rapid Screening and Mass Profiling of Naphthenic Acids Directly in Contaminated Aqueous Samples. *J. Mass Spectrom.* **2016**, *51* (1), 44−52.

(32) Woudneh, M. B.; Hamilton, M. C.; Benskin, J. P.; Wang, G.; McEachern, P.; Cosgrove, J. R. A Novel Derivatization-Based Liquid Chromatography Tandem Mass Spectrometry Method for Quantitative Characterization of Naphthenic Acid Isomer Profiles in Environmental Waters. *J. Chromatogr. A* **2013**, *1293*, 36−43, DOI: 10.1016/j.chroma.2013.03.040.

(33) Kaiser, N. K.; Savory, J. J.; McKenna, A. M.; Quinn, J. P.; Hendrickson, C. L.; Marshall, A. G. Electrically Compensated Fourier Transform Ion Cyclotron Resonance Cell for Complex Mixture Mass Analysis. *Anal. Chem.* **2011**, *83* (17), 6907−6910.

(34) Blakney, G. T.; Hendrickson, C. L.; Marshall, A. G. Predator Data Station: A Fast Data Acquisition System for Advanced FT-ICR MS Experiments. *Int. J. Mass Spectrom.* **2011**, *306* (2), 246−252.

(35) Xian, F.; Hendrickson, C. L.; Blakney, G. T.; Beu, S. C.; Marshall, A. G. Automated Broadband Phase Correction of Fourier Transform Ion Cyclotron Resonance Mass Spectra. *Anal. Chem.* **2010**, *82* (21), 8807−8812.

(36) Savory, J. J.; Kaiser, N. K.; McKenna, A. M.; Xian, F.; Blakney, G. T.; Rodgers, R. P.; Hendrickson, C. L.; Marshall, A. G. Parts-Per-Billion Fourier Transform Ion Cyclotron Resonance Mass Measurement Accuracy with a "Walking" Calibration Equation. *Anal. Chem.* **2011**, *83* (5), 1732−1736.

(37) McKenna, A. M.; Chacón-Patiño, M. L.; Weisbrod, C. R.; Blakney, G. T.; Rodgers, R. P. Molecular-Level Characterization of Asphaltenes Isolated from Distillation Cuts. *Energy Fuels* **2019**, *33* (3), 2018−2029.

(38) Kendrick, E. A Mass Scale Based on CH_2 = 14.0000 for High Resolution Mass Spectrometry of Organic Compounds. *Anal. Chem.* **1963**, *35* (13), 2146−2154.

(39) Hughey, C. A.; Hendrickson, C. L.; Rodgers, R. P.; Marshall, A. G.; Qian, K. Kendrick Mass Defect Spectrum: A Compact Visual Analysis for Ultrahigh-Resolution Broadband Mass Spectra. *Anal. Chem.* **2001**, *73* (19), 4676−4681.

(40) Ajaero, C.; Peru, K. M.; Hughes, S. A.; Chen, H.; McKenna, A. M.; Corilo, Y. E.; McMartin, D. W.; Headley, J. V. Atmospheric Pressure Photoionization Fourier Transform Ion Cyclotron Resonance Mass Spectrometry Characterization of Oil Sand Process-Affected Water in Constructed Wetland Treatment. *Energy Fuels* **2019**, *33* (5), 4420−4431.

(41) Wickham, H.; Averick, M.; Bryan, J.; Chang, W.; McGowan, L.; François, R.; Grolemund, G.; Hayes, A.; Henry, L.; Hester, J.; Kuhn, M.; Pedersen, T.; Miller, E.; Bache, S.; Müller, K.; Ooms, J.; Robinson, D.; Seidel, D.; Spinu, V.; Takahashi, K.; Vaughan, D.; Wilke, C.; Woo, K.; Yutani, H. Welcome to the Tidyverse. *J. Open Source Software* **2019**, *4* (43), No. 1686, DOI: 10.21105/joss.01686.

(42) Lemkau, K. L.; McKenna, A. M.; Podgorski, D. C.; Rodgers, R. P.; Reddy, C. M. Molecular Evidence of Heavy-Oil Weathering Following the M/V *Cosco Busan* Spill: Insights from Fourier Transform Ion Cyclotron Resonance Mass Spectrometry. *Environ. Sci. Technol.* **2014**, *48* (7), 3760−3767.

(43) Pan, Y.; Liao, Y.; Shi, Q. Variations of Acidic Compounds in Crude Oil during Simulated Aerobic Biodegradation: Monitored by Semiquantitative Negative-Ion ESI FT-ICR MS. *Energy Fuels* **2017**, *31* (2), 1126−1135.

(44) Su, S.; Dong, H.; Yu, G.; Hou, D.; Shi, Q.; Banat, I. M.; Wang, Z.; Gu, Y.; Zhang, F.; She, Y. Tracking Alterations of Alkyl Side Chains of N1 Species in Heavy Crude Oil after Anaerobic Biodegradation with Negative-Ion Electrospray Ionization Coupled with High-Field Fourier Transform Ion Cyclotron Resonance Mass Spectrometry. *Rapid Commun. Mass Spectrom.* **2019**, *33* (9), 875−882.

(45) Niles, S. F.; Chacón-Patiño, M. L.; Marshall, A. G.; Rodgers, R. P. Molecular Composition of Photooxidation Products Derived from Sulfur-Containing Compounds Isolated from Petroleum Samples. *Energy Fuels* **2020**, *34* (11), 14493−14504.

(46) Islam, A.; Cho, Y.; Yim, U. H.; Shim, W. J.; Kim, Y. H.; Kim, S. The Comparison of Naturally Weathered Oil and Artificially Photo-Degraded Oil at the Molecular Level by a Combination of SARA Fractionation and FT-ICR MS. *J. Hazard. Mater.* **2013**, *263*, 404−411.

(47) Schittmayer, M.; Birner-Gruenberger, R. Resolution Ladder for High-Resolution Mass Spectrometry. *Anal. Chem.* **2017**, *89* (18), 9611−9615.

(48) McKenna, A. M.; Williams, J. T.; Putman, J. C.; Aeppli, C.; Reddy, C. M.; Valentine, D. L.; Lemkau, K. L.; Kellermann, M. Y.; Savory, J. J.; Kaiser, N. K.; Marshall, A. G.; Rodgers, R. P. Unprecedented Ultrahigh Resolution FT-ICR Mass Spectrometry and Parts-Per-Billion Mass Accuracy Enable Direct Characterization of Nickel and Vanadyl Porphyrins in Petroleum from Natural Seeps. *Energy Fuels* **2014**, *28* (4), 2454−2464.

(49) Han, X.; Scott, A. C.; Fedorak, P. M.; Bataineh, M.; Martin, J. W. Influence of Molecular Structure on the Biodegradability of Naphthenic Acids. *Environ. Sci. Technol.* **2008**, *42* (4), 1290−1295.

(50) Hwang, G.; Dong, T.; Islam, M. S.; Sheng, Z.; Pérez-Estrada, L. A.; Liu, Y.; El-Din, M. G. The Impacts of Ozonation on Oil Sands Process-Affected Water Biodegradability and Biofilm Formation Characteristics in Bioreactors. *Bioresour. Technol.* **2013**, *130*, 269−277, DOI: 10.1016/j.biortech.2012.12.005.

(51) McKenzie, N.; Yue, S.; Liu, X.; Ramsay, B. A.; Ramsay, J. A. Biodegradation of Naphthenic Acids in Oils Sands Process Waters in an Immobilized Soil/Sediment Bioreactor. *Chemosphere* **2014**, *109*, 164−172.

(52) Zito, P.; Chen, H.; Podgorski, D. C.; McKenna, A. M.; Tarr, M. A. Sunlight Creates Oxygenated Species in Water-Soluble Fractions of Deepwater Horizon Oil. *J. Hazard. Mater.* **2014**, *280*, 636−643.

(53) Ajaero, C.; Meulen, I. V.; Simair, M. C.; le Roux, M.; Parrott, J.; Peru, K. M.; McMartin, D. W.; Headley, J. V. Developments in Molecular Level Characterization of Naphthenic Acid Fraction Compounds Degradation in a Constructed Wetland Treatment System. *Environments* **2020**, *7* (10), No. 89, DOI: 10.3390/environments7100089.

(54) Ahad, J. M. E.; Pakdel, H.; Gammon, P. R.; Siddique, T.; Kuznetsova, A.; Savard, M. M. Evaluating in Situ Biodegradation of 13C-Labelled Naphthenic Acids in Groundwater near Oil Sands Tailings Ponds. *Sci. Total Environ.* **2018**, *643*, 392−399.

(55) Alberts, M. E.; Wong, J.; Hindle, R.; Degenhardt, D.; Krygier, R.; Turner, R. J.; Muench, D. G. Detection of Naphthenic Acid Uptake into Root and Shoot Tissues Indicates a Direct Role for Plants in the Remediation of Oil Sands Process-Affected Water. *Sci. Total Environ.* **2021**, *795*, No. 148857.

(56) de Oliveira Livera, D.; Leshuk, T.; Peru, K. M.; Headley, J. V.; Gu, F. Structure-Reactivity Relationship of Naphthenic Acids in the Photocatalytic Degradation Process. *Chemosphere* **2018**, *200*, 180−190.

(57) Medeiros, D. C. C. D. S.; Chelme-Ayala, P.; El-Din, M. G. Sorption and Desorption of Naphthenic Acids on Reclamation Materials: Mechanisms and Selectivity of Naphthenic Acids from Oil Sands Process Water. *Chemosphere* **2023**, *326*, No. 138462, DOI: 10.1016/j.chemosphere.2023.138462.

(58) Janfada, A.; Headley, J. V.; Peru, K. M.; Barbour, S. L. A Laboratory Evaluation of the Sorption of Oil Sands Naphthenic Acids on Organic Rich Soils. *J. Environ. Sci. Health, Part A* **2006**, *41* (6), 985−997.

(59) Peng, J.; Headley, J. V.; Barbour, S. L. Adsorption of Single-Ring Model Naphthenic Acids on Soils. *Can. Geotech. J.* **2002**, *39* (6), 1419−1426.

(60) Han, X.; MacKinnon, M. D.; Martin, J. W. Estimating the in Situ Biodegradation of Naphthenic Acids in Oil Sands Process Waters by HPLC/HRMS. *Chemosphere* **2009**, *76* (1), 63−70.

(61) Alharbi, H. A.; Saunders, D. M. V.; Al-Mousa, A.; Alcorn, J.; Pereira, A. S.; Martin, J. W.; Giesy, J. P.; Wiseman, S. B. Inhibition of ABC Transport Proteins by Oil Sands Process Affected Water. *Aquatic Toxicol.* **2016**, *170*, 81−88.